



# Multipath error mitigation method considering NLOS signal for high-precision GNSS data processing

Xuan Zou<sup>1,2</sup> · Ruinan Fu<sup>1</sup> · Jian Tang<sup>1</sup> · Yawei Wang<sup>1</sup> · Xiaoyun Fan<sup>1</sup> · Zhiyuan Li<sup>1</sup> · Chenlong Deng<sup>1</sup> · Yangyang Li<sup>1</sup> · Weiming Tang<sup>1,3</sup>

Received: 31 May 2022 / Accepted: 13 June 2023 / Published online: 20 July 2023  
© The Author(s), under exclusive licence to Springer-Verlag GmbH Germany, part of Springer Nature 2023

## Abstract

The non-line-of-sight (NLOS) signal has different signal characteristics and error from multipath, and it may lead to significant errors in the Global Navigation Satellite System (GNSS) positioning at the centimeter to millimeter range. However, the current multipath error mitigation methods for carrier phase observations do not distinguish them effectively. The multipoint hemispherical grid model (MHGM) is a method to model the multipath error in the spatial domain. We detect the NLOS carrier signal at a static station by the three-dimensional environment data and evaluate the reduction effects of the MHGM on multipath and NLOS errors. In our experiments, the MHGM reduces both multipath and NLOS errors significantly for the double-differenced residuals of carrier phase observations. But after using MHGM, the accuracy of NLOS observation is still significantly lower than that of multipath. We determine the accuracy difference between multipath and NLOS observations of the station, and propose two improved strategies based on the original MHGM which is also called strategy 0: strategy 1 of eliminating NLOS signal and strategy 2 of reducing its weight in the GNSS data processing. Our kinematic positioning test indicates that with multiple satellite systems, strategies 1 and 2 improve the mean RMSE of positioning results by about 10% and 15–17%, respectively. With fewer satellite systems, strategy 1 of eliminating NLOS signals may lead to poor satellite geometry and cannot improve effectively, while strategy 2 of reducing the weight of NLOS signals is more robust and recommended.

**Keywords** GNSS · High-precision · Multipath · NLOS · MHGM

## Introduction

The Global Navigation Satellite System (GNSS) is widely used in various fields. Meanwhile, many industries and users also put forward higher requirements for GNSS navigation and positioning accuracy. In recent years, with the research on high-precision GNSS data processing by different scholars, some errors in GNSS positioning have been significantly mitigated, such as satellite clock error, and tropospheric and ionospheric errors. Meanwhile, since the multipath error is

highly related to the station environment, it is hard to be eliminated by universal models. Therefore, the multipath error has become one of the main error sources in high-precision GNSS data processing, which limits the application of GNSS in many cases (Lau and Cross 2007; Zhang et al. 2019).

In order to mitigate the influence of multipath effect, many measures have been taken: Choose the station position with good observation environment that avoids obstacles, reflectors and radiation sources as much as possible; use special hardware equipments, such as choke rings (Filippov et al. 1998) and antenna ground planes (Tatarnikov et al. 2005). In addition, the multipath error can also be mitigated by data processing algorithms. Among them, the sidereal filtering (SF) (Agnew and Larson 2007; Ragheb et al. 2007) and the lookup table (Cohen and Parkinson 1991) are widely used now. The SF method separates the multipath error according to the periodic repetition characteristics of the satellite orbit. However, different satellite orbit repetition

✉ Yawei Wang  
grcwongyw2016@whu.edu.cn

<sup>1</sup> GNSS Research Center, Wuhan University, 129 Luoyu Road, Wuhan 430079, China

<sup>2</sup> Hubei LuoJia Laboratory, 129 Luoyu Road, Wuhan 430079, China

<sup>3</sup> Collaborative Innovation Center of Geospatial Technology, 129 Luoyu Road, Wuhan 430079, China

periods make the SF method complicated, and its effect will be reduced if the sampling rates are sparse. The lookup table, multipath stacking maps (Fuhrmann et al. 2015) and multipath hemispherical map (MHM) (Dong et al. 2016) model the multipath error in the spatial domain. However, it is not accurate enough to correct the multipath error by using the average of observation residuals. By fitting the trend of multipath error in the hemispherical grid, Wang et al. (2019) further proposed the trend surface analysis-based multipath hemispherical map (T-MHM), and Lu et al. (2021) tested its performance in precision point positioning. In addition, Wang et al. (2020) proposed the multipoint hemispherical grid model (MHGM), which uses the double-differenced (DD) carrier phase observation residuals to model the multipath error. This method is applicable to different GNSS systems, different satellite constellations and various existing data processing modes of GNSS network solution.

Generally, we consider that the multipath effect is caused by the direct and reflected or diffraction signals of satellite entering the receiver antenna together. However, in densely built area or other complex environments with serious blocking, satellite signal that cannot be received directly due to obstructions can also enter the receiver antenna independently through reflection or diffraction, which is called non-line-of-sight (NLOS) signal (Bradbury et al. 2007; Groves and Adjrjad 2017). On the one hand, the NLOS signal has different signal characteristics from multipath effect. Multipath effect is generated by the superposition of direct, reflected and diffraction signals, while NLOS signal does not contain direct signal (Hsu 2018).

On the other hand, NLOS signal has different ranging error from multipath effect. The multipath error might be positive or negative (Groves and Adjrjad 2017). For pseudorange observation, the reflected signal distorts the code correlation process in the receiver, and the resulting ranging error can be up to half a code chip (Bradbury et al. 2007). For the carrier phase observation, multipath effect offsets the carrier phase through the additional path delay of the reflected signal, and the theoretical maximum ranging error could reach one-fourth of the carrier wavelength (Hofmann-Wellenhof et al. 2008). However, the pseudorange measurement error caused by NLOS signal is always positive and equals to the additional path length of the reflected signal compared with the blocked direct signal, which usually ranges from several meters to tens of meters (Jiang and Groves 2014). For the ranging error of NLOS carrier signal, some researchers said that it is similar to the NLOS pseudorange error (Groves and Jiang 2013), but there is little research on it at present.

In order to detect and mitigate the NLOS signal reception, researchers have proposed many different methods. As a hardware-based approach, the dual-polarization antenna technique (Jiang and Groves 2014) combines coaxial right-hand circularly polarized (RHCP) and left-hand circularly

polarized (LHCP) sensitive antennas. By comparing the output measurements of the two types of antennas, the dual-polarization antenna can distinguish NLOS signal, multipath signal and pure direct signal effectively. However, depending on special hardware equipment, dual-polarization antenna technique is not a universal method. In terms of data processing algorithms, the consistency checking (Groves and Jiang 2013) is a method to detect NLOS and multipath signals based on the consistency among observations, which needs no additional hardware. When most signals are received through the direct path, the NLOS and multipath signals can be successfully detected by consistency checking method. However, in the densely built area with serious NLOS signal reception and multipath interference, consistency checking method will become unreliable. In addition, Hsu et al. (2015) proposed that the vector tracking algorithm can also mitigate the influence of NLOS and multipath signals, and tested its performance under the situation of long-path-delay NLOS signal reception. The vector tracking algorithm combines tracking GNSS signals with calculating the user positions, which is suitable for both static and dynamic scenes, but they only tested NLOS pseudorange signal.

With the rapid development and wide application of three-dimensional (3D) building models, they are increasingly used to assist navigation and improve positioning accuracy in densely built area. 3D building models combined with user's location can determine satellite visibility, which can be used to detect NLOS signal reception. However, memory space required to store the massive data of 3D building models, and the huge amounts of calculation consumed by testing satellite visibility frequently, makes it difficult to be applied in practice. Wang et al. (2012, 2013) proposed building boundary method for determining satellite visibility: According to 3D building models and user's location, generate the building boundaries from user's perspective in advance, which are expressed by the elevation angle of the building edge at each azimuth. Therefore, satellite visibility can be determined by comparing the elevation angle of the satellite with building boundary at the same azimuth. The building boundary method significantly reduces the large storage space and calculation, which is required by using the original data of 3D building models directly. However, if there is space below the building boundary that allows satellite signal to pass through, such as overhead bridge, arch and other building structures, the building boundary method may not predict satellite visibility correctly.

Although NLOS signal reception is gradually regarded as one of the error sources which cannot be ignored in GNSS positioning, at present, most studies on NLOS signal are about pseudorange observations. In the GNSS positioning at the centimeter to millimeter range, the NLOS signal reception may lead to significant errors, and its error characteristics are different from multipath. However, the current

multipath error mitigation methods for carrier phase observations do not effectively distinguish multipath and NLOS signals.

We focus on improving the accuracy of GNSS data processing by optimizing the multipath error mitigation method. First, the method for detecting NLOS carrier signal at the static station by 3D environment data is proposed. Afterward, we propose two improved strategies based on the original MHGM, i.e., strategy 0: eliminating NLOS signal or reducing its weight. Then we introduce the experimental design. In the experiment part, we evaluate the MHGM's reduction effects on DD carrier phase residuals, and compare the accuracy difference between multipath and NLOS observations after using MHGM. In the positioning test, we compare the two improved strategies with strategy 0, to test the effectiveness of the multipath error mitigation methods we proposed. Finally, some conclusions and suggestions are summarized.

### NLOS carrier signal detection by 3D environment data

Referring to the building boundary method, we transform 3D environment data to the hemisphere of the static station for presentation. Based on this, we can determine satellite visibility and detect the NLOS carrier signal. The hemisphere at the station is established with the phase center of the antenna as the origin and is divided into grids according to the azimuth and elevation angles. The azimuth angle range of the hemisphere is set from 0° to 360°, and the elevation angle range is set from  $E_0$  to  $E_1$ , where  $E_0$  is generally set as the satellite cutoff elevation angle. For the hemispherical grid, the division intervals of azimuth and elevation angles are set to  $d_A$  and  $d_E$ , respectively, which indicate the density of the grid division. An example of the grid division of a hemisphere is given below ( $E_0 = 20^\circ, E_1 = 80^\circ, d_A = d_E = 20^\circ$ ).

In order to obtain the 3D environment data around the station, including buildings, trees and other objects that may block satellite signals, techniques such as close-range photogrammetry and 3D light detection and ranging (LiDAR) can be used. Taking 3D LiDAR as an example, it collects 3D environment data in the form of point cloud. According to the coordinate of a laser point, we can calculate its azimuth and elevation angles at the station, and map it to the corresponding grid cell of the hemisphere as shown in Fig. 1. Then the number of laser points mapped to each grid cell is recorded and expressed as  $N$ . Due to the limitation of 3D LiDAR itself, the influence of the measurement environment and other factors, the point cloud inevitably has noise points (Deng et al. 2016). In order to avoid the influence of noise points on determining satellite visibility, we set an empirical value  $N_0$  as the minimum threshold for the number of laser

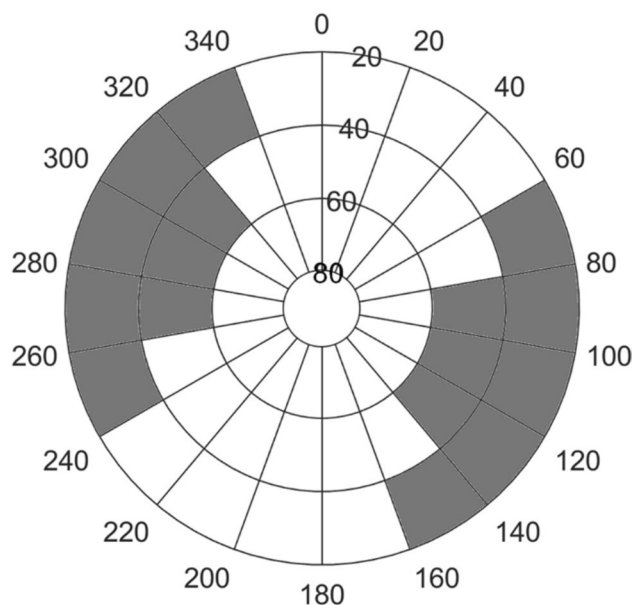


Fig. 1 An example of the grid division of a hemisphere. All the grid cells are filled with gray or white to indicate whether there are obstructions in the corresponding directions

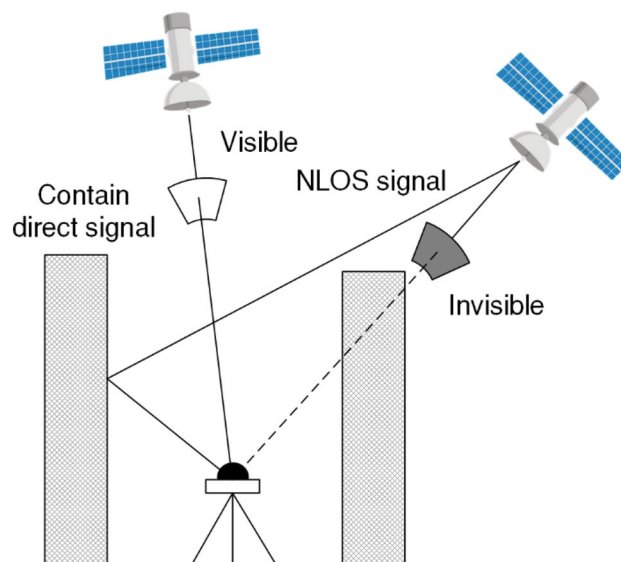


Fig. 2 Detecting NLOS signal by transforming 3D environment data to the hemisphere of the station

points, to judge whether there are obstructions in the direction of the grid cell, which is indicated by gray and white colors as shown in Fig. 1.

Figure 2 further shows the specific details of detecting NLOS signal by transforming 3D environment data to the hemisphere of the station. First the azimuth and elevation angles of the satellite is calculated according to its coordinate, then its position on the hemisphere can be determined.

If the number  $N$  of laser points in the direction of corresponding grid cell is fewer than  $N_0$ , it indicates that there is no obstruction in the grid cell's direction (white grid cell, as shown in Fig. 2), which means that the satellite signal contains direct signal. Conversely, if the number  $N$  of laser points is greater than  $N_0$ , it indicates that there are obstructions in the grid cell's direction (gray grid cell, as shown in Fig. 2), which means that the satellite signal is NLOS signal. For the hemispherical grid in this section, its division intervals  $d_A$  and  $d_E$  are determined according to the number of laser points and surrounding obstructions and can be different from the MHGM in the next section.

### Multipath error mitigation method considering NLOS signal

As mentioned in Introduction, we further process the NLOS signal based on the MHGM. Therefore, it is necessary to introduce the principle of MHGM in detail. After that, the improved multipath error mitigation method strategies considering NLOS signal are presented.

#### Multipoint hemispherical grid model

Assuming that the multipath effect is caused by a single reflected signal, the error  $M$  of carrier phase observation can be described by the following formula (Elosegui et al. 1995)

$$M = \frac{\lambda}{2\pi} \tan^{-1} \frac{\alpha \sin \left( 4\pi \frac{H}{\lambda} \sin \varepsilon \right)}{1 + \alpha \cos \left( 4\pi \frac{H}{\lambda} \sin \varepsilon \right)} \quad (1)$$

where  $\lambda$  is the wavelength of satellite signal,  $\alpha$  is the attenuation coefficient of the reflected signal,  $H$  is the antenna height and  $\varepsilon$  is the incident angle of reflected signal. According to Eq. (1), for the satellite signal with certain wavelength, the multipath error depends on the attenuation coefficient and the spatial relationship among satellite, receiver antenna and reflector. In other words, if the receiver antenna and surrounding observation environment remain unchanged, the multipath errors caused by different satellite signals of the same frequency only depend on their positions in the sky, but have nothing to do with the observation time or a specific satellite.

Based on the characteristics of the multipath error in the spatial domain described above, Wang et al. (2020) proposed the MHGM. The MHGM is also established on the hemisphere at the station, with the phase center of the antenna as the origin. Unlike the grid division scheme in the above section, the MHGM sets the model parameters at the grid points, representing the multipath errors caused by the satellite signals with the azimuth and elevation angles

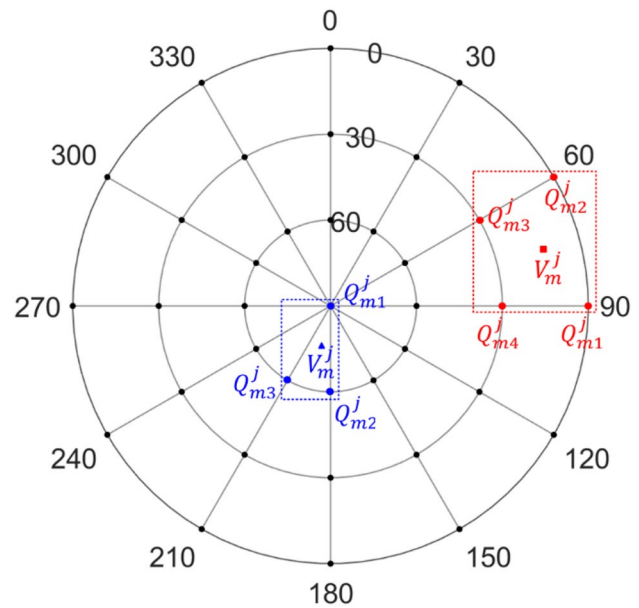


Fig. 3 Distribution of the hemispherical grid points. The multipath error  $V_m^j$  can be expressed by the model parameters of four or three adjacent grid points

corresponding to the grid points. Taking satellite  $j$  and station  $m$  for an example, satellite  $j$  is projected on the hemisphere at station  $m$  along its signal propagation direction, and its elevation and azimuth angles are  $(E, A)$ . Furthermore, the spatial relationship between the pierce point of satellite  $j$  and the adjacent grid points is determined, while the grid points adjacent to the pierce point may be four or three as shown in Fig. 3. According to the plane interpolation method, the multipath error  $V_m^j$  of satellite  $j$  at station  $m$  can be described by the model parameters at adjacent grid points.

If the pierce point of satellite  $j$  has four adjacent grid points, as shown on the part within red dashed line in Fig. 3, it is assumed that the model parameters of the four grid points are  $Q_{m1}^j, Q_{m2}^j, Q_{m3}^j, Q_{m4}^j$ , while the elevation and azimuth angles of them are  $(E_1, A_1), (E_2, A_2), (E_2, A_2), (E_2, A_1)$ , respectively. According to the bilinear interpolation method, the multipath error  $V_m^j$  of satellite  $j$  at station  $m$  can be expressed as:

$$V_m^j = \omega_{m1}^j Q_{m1}^j + \omega_{m2}^j Q_{m2}^j + \omega_{m3}^j Q_{m3}^j + \omega_{m4}^j Q_{m4}^j \quad (2)$$

where  $\omega_{m1}^j = \frac{(E_2-E)(A_2-A)}{(E_2-E_1)(A_2-A_1)}, \omega_{m2}^j = \frac{(E_2-E)(A-A_1)}{(E_2-E_1)(A_2-A_1)},$   
 $\omega_{m3}^j = \frac{(E-E_1)(A-A_1)}{(E_2-E_1)(A_2-A_1)}, \omega_{m4}^j = \frac{(E-E_1)(A_2-A)}{(E_2-E_1)(A_2-A_1)}.$

Similarly, if the pierce point of satellite  $j$  has three adjacent grid points, as shown on the part within blue dashed line in Fig. 3, it is assumed that the model parameters of the three grid points are  $Q_{m1}^j, Q_{m2}^j$  and  $Q_{m3}^j$ , while the elevation



and azimuth angles of them are  $(E_1, A_1)$ ,  $(E_2, A_2)$  and  $(E_2, A_3)$ , respectively. According to the bilinear interpolation method, the multipath error  $V_m^j$  of satellite  $j$  at station  $m$  can be expressed as:

$$V_m^j = (1 - u - v)Q_{m1}^j + uQ_{m2}^j + vQ_{m3}^j \tag{3}$$

where  $u = \frac{(A-A_1)(E_2-E)-(E-E_1)(A_3-A_1)}{(E_2-E_1)(A_3-A_1)}$ ,  $v = \frac{(A_2-A_1)(E-E_1)-(E_2-E_1)(A-A_1)}{(E_2-E_1)(A_3-A_1)}$ .

In order to eliminate other errors in GNSS carrier phase observations, we chose the DD observation model. Taking stations  $m, n$  and satellites  $j, k$  for an example, making difference between observations at stations  $m$  and  $n$  can eliminate satellite clock error, most of the satellite orbit, ionospheric and tropospheric errors, while making difference between observations of satellites  $j$  and  $k$  can further eliminate the receiver clock error. Therefore, we consider that the DD carrier phase observation residuals in the ambiguity-fixed periods only contain multipath errors, NLOS signal errors and observation noises. We call these residual errors as multipath error collectively.

According to Eq. (2) or (3), the multipath error  $V_m^j$  of satellite  $j$  at station  $m$  is described by the model parameters of adjacent grid points. Similarly, the other three multipath errors of satellite  $j$  and  $k$  at station  $m$  and  $n$  are generated, then the DD residual  $s$  can be expressed as:

$$s = (V_m^j - V_m^k) - (V_n^j - V_n^k) \tag{4}$$

According to the above observation equation, using the DD residuals of different periods, satellites and stations, the model parameters at all grid points are solved by least-square estimation. When applying MHGM, use the model parameters of adjacent grid points to calculate the multipath error of the satellite at the station, and then, correct the observation.

### Improved strategies of multipath error mitigation considering NLOS signal

As mentioned in the above section, for the DD carrier phase observation in the ambiguity-fixed period, we use 3D environment data to detect whether its original observations are NLOS signals. Based on this, we can classify the DD observations and then compare the root mean square (RMS) of various DD residuals (see the section of error characteristics analysis for more details). The test results show that: After using MHGM, the RMS of DD residuals with NLOS signals is significantly reduced, but still higher than that without NLOS signals, which means that the accuracy of NLOS observation is still lower than that of multipath observation. We further evaluate the accuracy difference between NLOS and multipath observations, and then calculate the scale factor  $k$  between them according to the propagation of uncertainty.

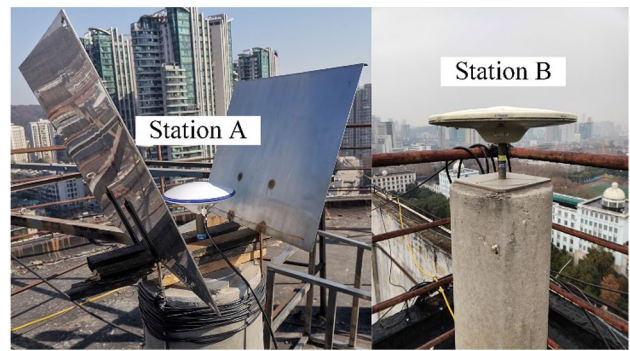


Fig. 4 Observation environments of stations A and B

Table 1 Hardware specifications of stations A and B

| Station             | A                    | B                   |
|---------------------|----------------------|---------------------|
| Receiver            | Septentrio PolaRx5TR | PANDA PD318         |
| Antenna             | HG-GOYH7151          | Trimble TRM55971.00 |
| With baffles or not | Yes                  | No                  |

Therefore, based on the original MHGM, i.e., strategy 0, we propose the following two improved strategies: Strategy 1: By eliminating the NLOS observations, do not allow them to participate in multipath error modeling and subsequent GNSS data processing. Strategy 2: According to the scale factor  $k$ , appropriately reduce the weight of NLOS observations in GNSS data processing. In the positioning test section, we compare the two improved strategies with strategy 0 to verify the effectiveness of the proposed multipath error mitigation methods. In addition, the method of detecting NLOS signal by 3D environment data is not limited to MHGM, but also applicable to SF, MHM and other multipath error mitigation methods.

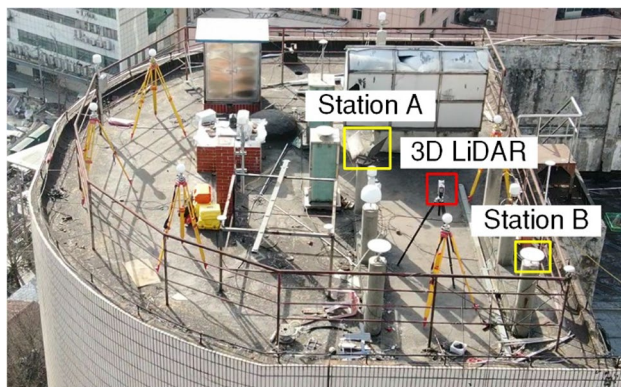
### Experimental design

We set up two stations A and B on the top floor of the Academic Experiment Building at Wuhan University. Two metal baffles were mounted in the northwest and southeast of station A, to simulate a strong multipath and NLOS environment. Station B was in the normal condition, and the multipath effect and NLOS signal reception were very weak. The observation environments of stations A and B are shown in Fig. 4, and the hardware specifications of them used in the experiment are shown in Table 1.

During days 15–30 of 2021, the carrier phase observation data of GPS, BDS and Galileo systems for 16 days were collected at stations A and B, with the sampling interval of 1 s. The antennas of the two stations and the surrounding environment remained unchanged. Again, theoretically,

**Table 2** Models and parameters for data processing

| Parameter            | Model   |
|----------------------|---|
| Signal frequency     | GPS L1 + BDS B1 + Galileo E1                      |
| Cutoff elevation     | 7 degrees   |
| Estimator            | Least square method                               |
| Observation weight   | Satellite elevation                               |
| Phase center pattern | igs14.atx   |
| Tropospheric delay   | GPT2 + Saastamonien + GMF                         |
| Satellite clock      | Broadcast + Process                               |
| Satellite orbit      | Broadcast   |
| Receiver clock       | Estimated + White noise                           |
| Station displacement | Solid earth tide + Pole tide + Ocean tide loading |
| Terrestrial frame    | ITRF2020  |

**Fig. 5** Collecting environment data around station A by 3D LiDAR

different satellite signals with the same frequency from the same hemispherical position generate same multipath errors at the static station (Dong et al. 2016). According to the frequency setting of GNSS, the frequencies of GPS's L1 and Galileo's E1 signals are both 1575.420 MHz, so these observations can be used together to establish the MHGM. In addition, BDS's B1 frequency is 1561.098 MHz and very close to them, so it is also taken into account (Tang et al. 2021).

The Positioning and Navigation Data Analyst (PANDA) software is used for data processing, which is the IGS Analysis Center software platform. Under the data processing mode of GNSS network solution of PANDA software, the DD observation residuals of different periods, satellites and stations are obtained and used for modeling the MHGM. The models and parameters used in the data processing are listed in Table 2.

We set up a FARO 3D LiDAR on the top of the building and collected the environment data around station A from different angles as shown in Fig. 5. The original laser point

cloud is in the space rectangular coordinate system, which is defined by the 3D LiDAR.

By collecting coordinates of the feature points and using the seven-parameter coordinate transformation method, the laser point cloud was converted to the topocentric coordinate system. According to the method of detecting NLOS carrier signal by 3D environment data, we mapped the laser points to the hemisphere of station A and recorded the number of laser points in each grid cell for detecting the NLOS signal. Here for the hemisphere of station A, set  $E_0=0^\circ$ ,  $E_1=89^\circ$ ,  $d_A=d_E=1^\circ$ , and set the minimum threshold  $N_0$  for the number of laser points to 5. The workflow diagrams of determining the obstructions around station using 3D LiDAR are shown in Fig. 6.

### Analysis on error characteristics of multipath and NLOS signals

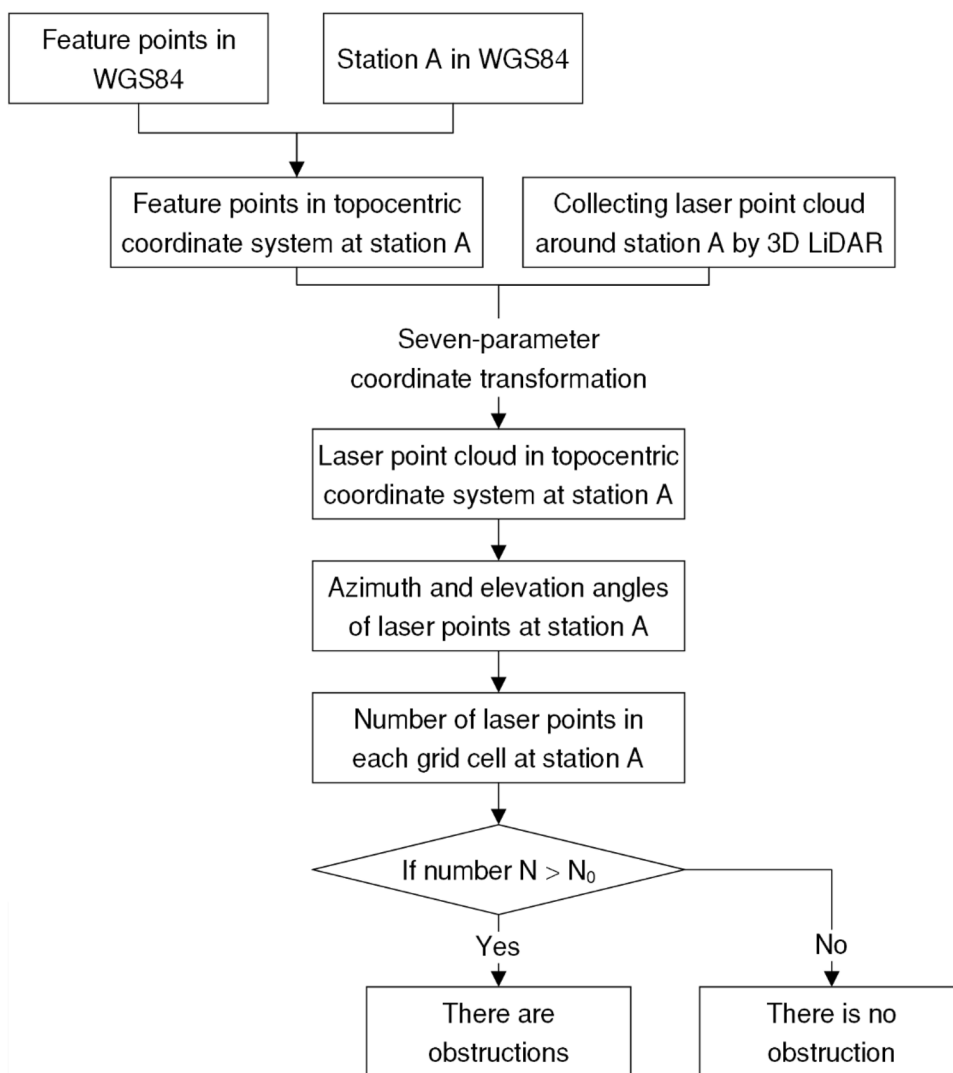
This section evaluates the MHGM's reduction effects on DD carrier phase residuals first. Then we analyze the accuracy difference between multipath and NLOS observations after using MHGM. Finally, according to the accuracy difference between them, the strategies of improved MHGM are proposed.

### Evaluation of MHGM's reduction effects on DD carrier phase residuals

First we fix the coordinates of stations A and B and obtain the DD carrier phase residuals. For the MHGM in this experiment, the elevation angle range is set from  $5^\circ$  to  $85^\circ$ , and the division intervals of azimuth and elevation angles are both set to  $2^\circ$ . Considering the different orbital repetition periods of satellites, we establish the MHGM based on the first 10-day observation data in this experimental period and use the last 6-day observation data for verification.

Under the condition with and without using MHGM, we calculate the DD residuals of each epoch in the ambiguity-fixed periods, respectively. In order to evaluate the reduction effects of MHGM on multipath and NLOS errors, use the method of detecting NLOS carrier signal by 3D environment data, so as to detect whether the undifferenced observations of station A are NLOS signals; then, divide the DD observations into two categories: category A of DD observation with only multipath signals but without NLOS signals and category B of DD observation with both multipath signals and NLOS signals, and their residuals: category A of DD residual and category B of DD residual. Under the condition with and without using MHGM, we calculate the RMS of the above two categories of DD residuals, respectively, by days and divide the experimental period into modeling days

**Fig. 6** Workflow diagrams of using 3D LiDAR to determine the obstructions around station



(the first 10 days) and verification days (the last 6 days) for statistic as shown in Fig. 7.

Without MHGM, the RMS of category A of DD residuals is very stable in the experimental period, and its mean value is 10.0 mm, while the RMS of category B of DD residuals is unstable, and its mean value is 35.1 mm. It indicates that the magnitude of NLOS error is much larger than that of multipath error, and the numerical stability of NLOS error is weaker than that of multipath error. With MHGM, the mean RMS of category A of DD residuals is 3.1 mm, which is 68.6% lower than that without MHGM; the mean RMS of category B of DD residuals is 6.7 mm, which is 80.9% lower than that without MHGM. The experimental results show that MHGM can mitigate not only multipath error, but also most NLOS error.

The modeling results of MHGM at station A are shown in Fig. 8. Large areas with azimuth angles of about 70°–160° and 250°–330° show high model values, which is consistent

with the orientation of the metal baffles mounted at station A as shown in Fig. 4. Theoretically, the direct signal of satellite cannot pass through the metal baffles, but there are observation residuals from these directions to participate in the modeling, and their model values are greater than 0. This indicates that station A did receive NLOS signals and their errors are positive, which is consistent with the theoretical error characteristics of NLOS signal, and further proves that MHGM can model NLOS error. In addition, it is noted that the model values in the area with azimuth angle about 300° at the bottom of the metal baffle are negative, but there are no observations from these directions. This is because there are constraints among model parameters of adjacent grid points. Therefore, when solving the MHGM by the least-square estimation, these grid points will have abnormal estimation values. However, this basically does not affect the reduction effects of MHGM.



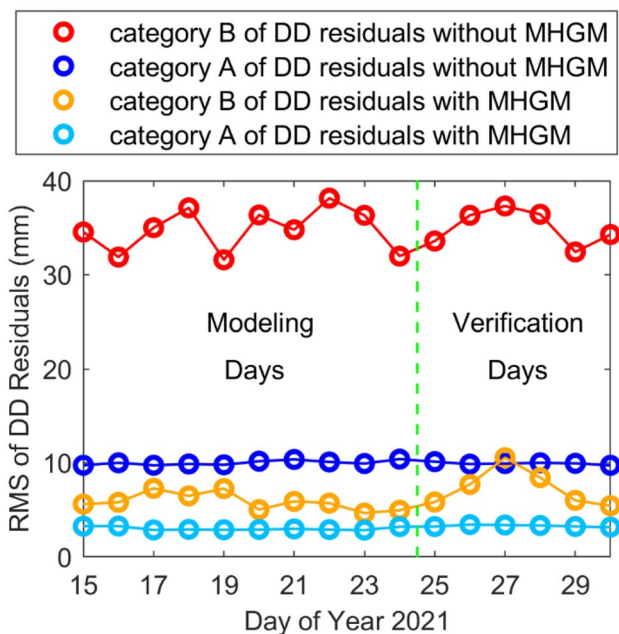


Fig. 7 RMS of the two categories of DD residuals with and without MHGM

Besides, Fig. 8 also displays the region of obstructions determined by 3D environment data in the form of dot matrix, to show the filtering effect of threshold  $N_0$  on laser points. The red dot matrix represents the region where the number of laser points is greater than the threshold  $N_0$ , while the purple dot matrix represents the region where the number of laser points is fewer than the threshold  $N_0$ . It should be noted that the dot matrix here only represents the region, but not the real laser points.

### Accuracy difference between the multipath and NLOS observations after using MHGM

As shown in Fig. 7, after using MHGM, the RMS of category B of DD residuals is still higher than that of category A, which indicates that the accuracy of NLOS observation is still lower than that of multipath observation. Next according to the number of undifferenced NLOS signals of station A, category B of DD observations is further divided into the following two categories: category BI of DD observation with one NLOS signal and three multipath signals; and category BII of DD observation with two NLOS signals and two multipath signals. With MHGM, we calculate the RMS of category A, category BI and category BII of DD residuals, respectively, by days, and the results in modeling days are shown in Fig. 9.

With MHGM, the RMS of both category BI and category BII of DD residuals is higher than that of category A in the modeling days. The mean RMS of category A of DD residuals is 3.0 mm; and the mean RMS of category BI of DD residuals is 6.0 mm, which is about twice that of category A, while the mean RMS of category BII of DD residuals is 7.6 mm, which is about 2.5 times that of category A. Then according to the propagation of uncertainty, we quantitatively evaluate the accuracy difference between multipath and NLOS observations.

It is assumed that when the ambiguity is fixed and other errors are corrected (including using MHGM), the root mean square error (RMSE) of NLOS observations is still several times that of multipath observations, i.e.,

$$m_{\text{NLOS}} = k \times m_{\text{multipath}} \tag{5}$$

where  $m_{\text{NLOS}}$  is the RMSE of NLOS observations;  $m_{\text{multipath}}$  is the RMSE of multipath observations; and  $k$  is the scale

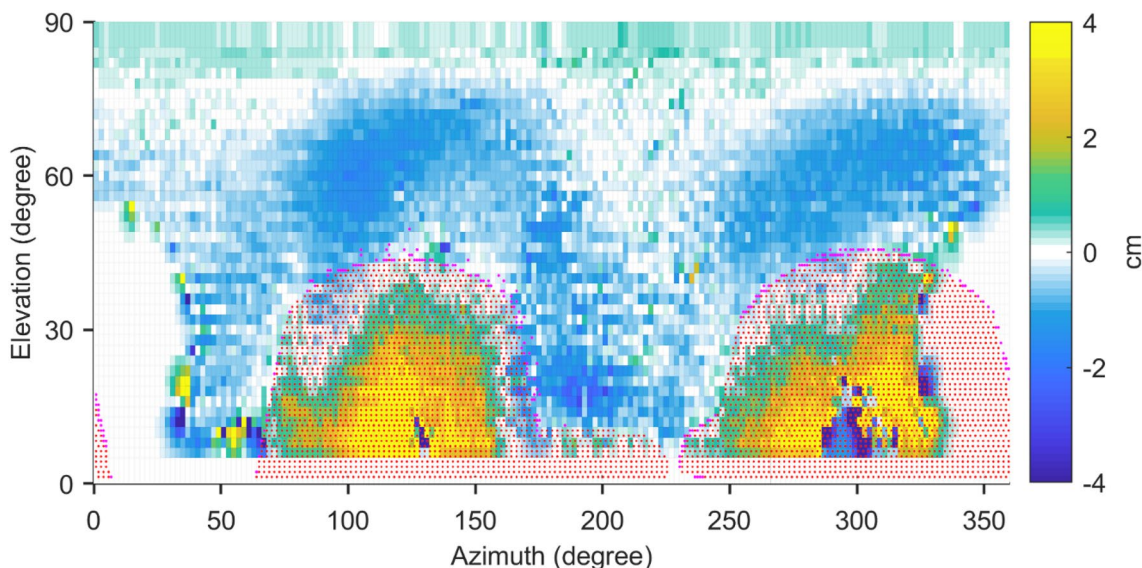


Fig. 8 Modeling results of MHGM at station A. Dot matrix represents the region of obstructions determined by 3D environment data



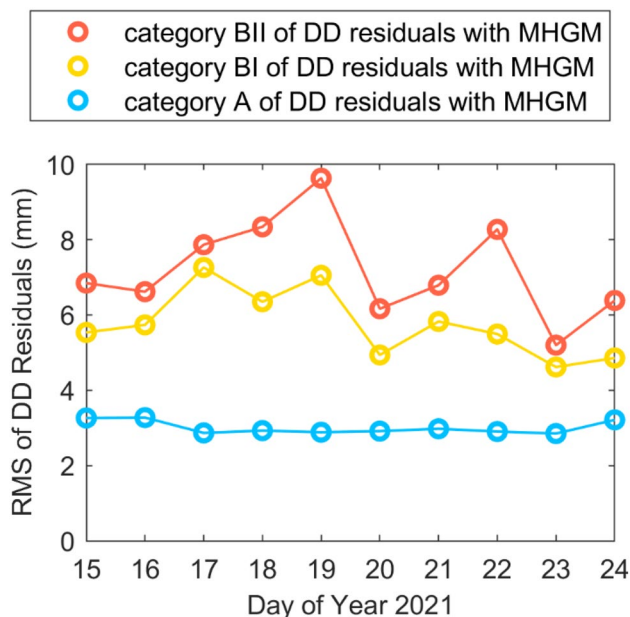


Fig. 9 RMS of the three categories of DD residuals with MHGM

factor that represents the accuracy difference between multipath and NLOS observations.

According to the propagation of uncertainty, the RMSE of category A of DD observations, namely  $m_A$ , is expressed as:

$$m_A = 2 \times m_{\text{multipath}} \tag{6}$$

And the RMSE of category BI of DD observations, namely  $m_{BI}$ , is expressed as:

$$m_{BI} = \sqrt{3 \times m_{\text{multipath}}^2 + m_{\text{NLOS}}^2} = \sqrt{3 + k^2} \times m_{\text{multipath}} \tag{7}$$

Similarly, the RMSE of category BII of DD observations, namely  $m_{BII}$ , is expressed as:

$$m_{BII} = \sqrt{2 + 2 \times k^2} \times m_{\text{multipath}} \tag{8}$$

We use the RMS of various observation residuals as the RMSE of these observations and obtain  $k \approx 3.5$  by combining Eqs. (6), (7) and (8). It means that after using MHGM, the RMSE of NLOS observations is still about 3.5 times that of multipath observations. In addition, it should be noted that the scale factor  $k$  obtained here is only applicable to describing the situation of station A.

### Strategies of improved MHGM

Considering the accuracy difference between multipath and NLOS observations, we propose two improved strategies based on strategy 0:

Strategy 1: In the modeling stage, the NLOS signals of station A are detected and eliminated first. Only multipath observation residuals are reserved for solving MHGM to improve its accuracy and effectiveness. In the GNSS data processing stage, NLOS observations are also detected and eliminated first, and then use the MHGM without NLOS signals to correct other multipath observations. The workflow diagram of strategy 1 is displayed in Fig. 10a.

Strategy 2: In the modeling stage, use all DD observation residuals in the ambiguity-fixed periods to establish MHGM. In the GNSS data processing stage, use MHGM to correct all observations first, and then, detect the NLOS signals at station A. After using MHGM, the RMSE of NLOS observations is still  $k$  times that of multipath observations, which indicates that the variance of NLOS observations is  $k^2$  times that of multipath observations. Therefore, based on the original method of determining weight by the elevation angle, the weight of NLOS observations is reduced to  $1/k^2 \approx 0.08$  of the previous one, while multipath observations keep their original weight. The workflow diagram of strategy 2 is displayed in Fig. 10b.

### Positioning test

We use the observation data in modeling days to establish MHGM. Strategies 0 and 2 use the same MHGM as that in the MHGM’s reduction effects evaluation section, while strategy 1 use the MHGM without NLOS signals, and other settings are the same. The observations of GPS, BDS, Galileo systems and L1/B1/E1 frequencies in extrapolation days are used for positioning test under the real-time kinematic (RTK) processing mode. Station A is set as the rover station and station B as the reference station, and the interval of positioning solution is set as 1 s. First we calculate the coordinates of station A under the above three strategies by days and take the average coordinates as the reference values. Then we solve the positioning results of station A under RTK mode and calculate the coordinate errors in the north, east and up directions. The RMSE of positing results in each direction is calculated in days as shown in Fig. 11.

Compared with strategy 0, the RMSE of station A under strategies 1 and 2 is generally reduced. In the extrapolation days, only the RMSE under strategy 1 in the north and east directions on day 26 is slightly higher than that under strategy 0. The mean RMSE under strategy 0 in the north, east and up directions is 1.33 mm, 1.42 mm and 4.92 mm, respectively; the mean RMSE under strategy 1 in the north, east and up directions is 1.20 mm, 1.25 mm and 4.37 mm, and improved by 9.7%, 10.7% and 11.0%, respectively, compared with strategy 0; the mean RMSE under strategy 2 in the north, east and up directions is 1.14 mm, 1.18 mm and 4.04 mm, and improved by 14.2%, 16.2% and 17.3%, respectively, compared with strategy 0. In general, the improvements of mean RMSE under strategy 2 are higher than that under strategy 1.

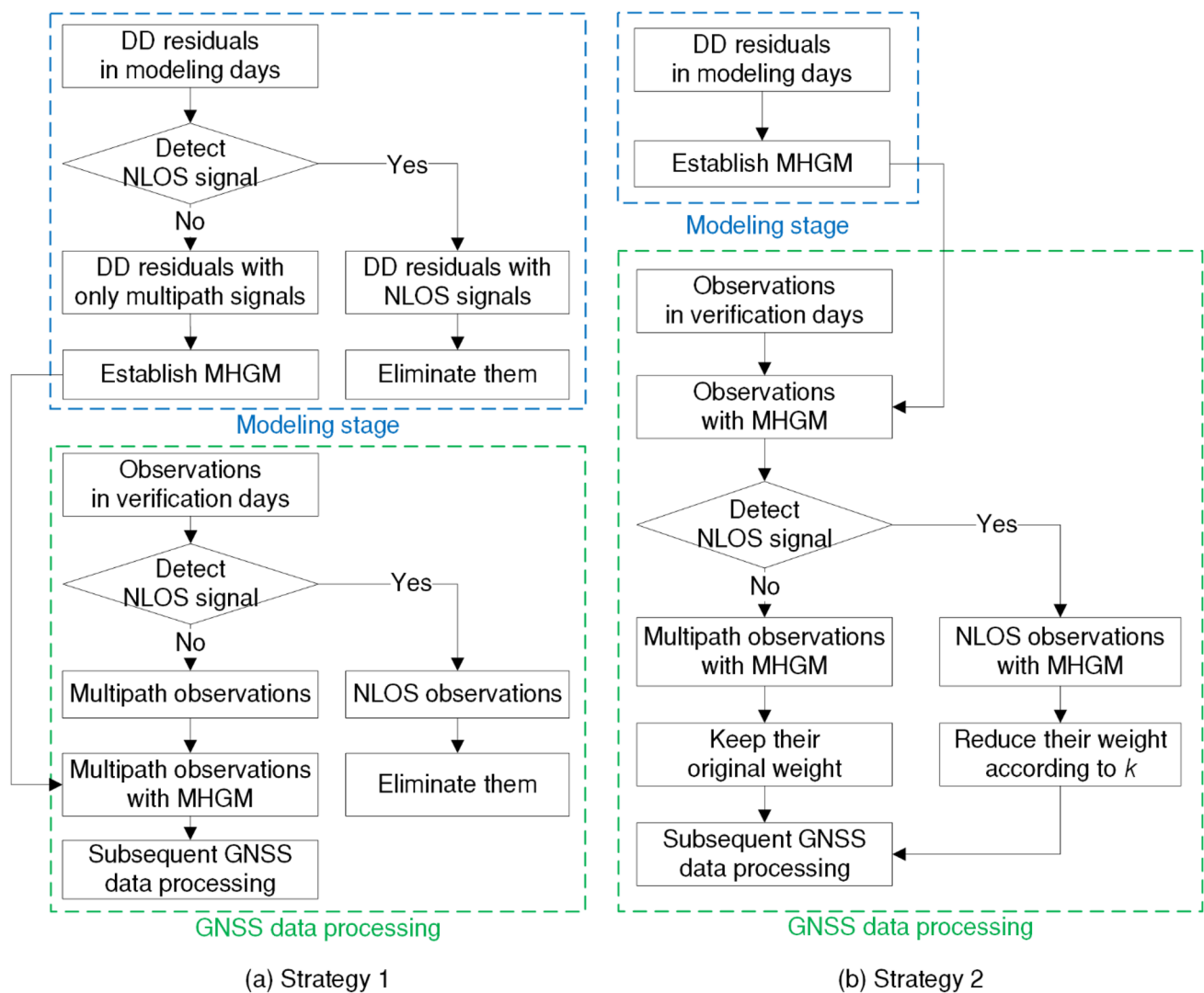


**Fig. 10** Workflow diagrams of the two strategies of improving the MHGM. Strategy 1 eliminates the NLOS signals, while strategy 2 reduces their weight

The statistical results shown in Fig. 11 are based on GPS, BDS and Galileo observations, and the number of available satellites is sufficient. In addition, we also concern about the performance of strategies 1 and 2 with fewer available satellites. Therefore, with the GPS-only, BDS-only and GPS plus BDS observations, the mean RMSE under the above three strategies is calculated in the horizontal and vertical directions, respectively. Under different satellite systems, we calculate the improvements of mean RMSE under strategies 1 and 2 compared with strategy 0 and the mean number of available satellites in each epoch.

As shown in Table 3, with GPS, BDS and Galileo observations, the mean number of available satellites in each epoch is 32.8. Compared with strategy 0, the improvements of strategy 1 in the horizontal and vertical directions are about 10%, while the improvements of strategy 2 are about 15–17%. With GPS plus BDS, BDS-only and GPS-only observations, the mean

numbers of available satellites are reduced to 27.4, 19.0 and 8.4, respectively, and the improvements of strategies 1 and 2 are also reduced. Among them, strategy 1 has no obvious improvements and even performs worse than strategy 0. Especially with the GPS-only observation, the mean RMSE under strategy 1 in the horizontal direction is 27.7% higher than that under strategy 0. This shows that with multiple satellite systems, strategy 1 has a certain improvement compared with strategy 0; however, with fewer satellite systems, strategy 1 of eliminating NLOS signals may lead to poor satellite geometry and cannot improve effectively (Groves and Jiang 2013; Xin et al. 2022). With observations of double systems or single system, the improvement of strategy 2 in the horizontal direction is reduced to about 5–8%, while the improvement in the vertical direction still remains 10–15%. This indicates that compared with strategy 1, strategy 2 of reducing the weight of NLOS signals is more robust.

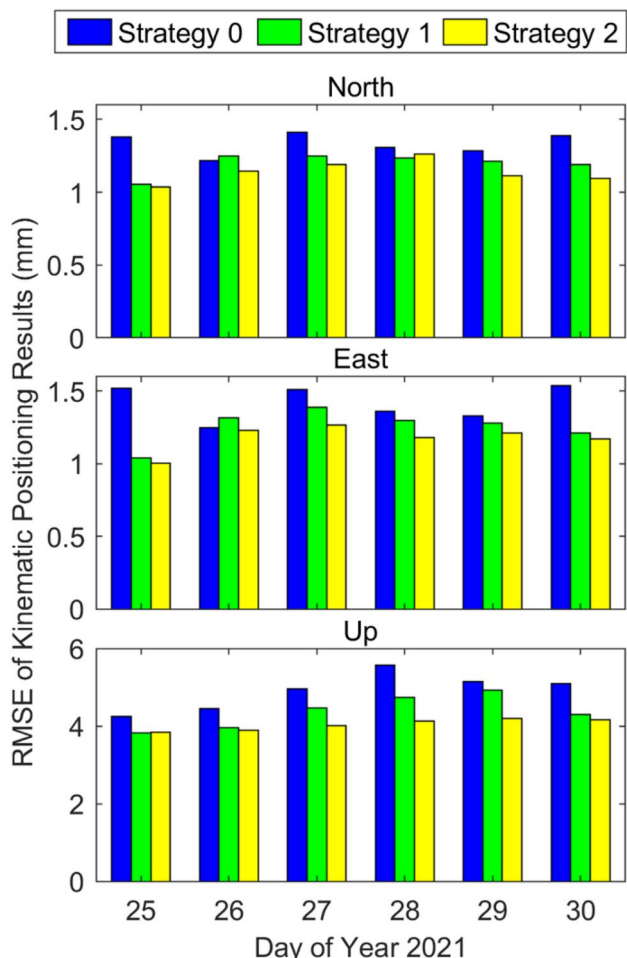


Fig. 11 RMSE of kinematic positioning results of station A in three directions

### Conclusion

NLOS signal has different error characteristics from multipath and may lead to significant errors in the GNSS positioning at the centimeter to millimeter range. However, the current multipath error mitigation methods for carrier phase observations

do not effectively distinguish multipath and NLOS signals. We collected the environment data around a static station and mapped it to the hemisphere of the station so as to detect the NLOS carrier signal.

The experimental analysis in the section of error characteristics analysis indicates that: Without using MHGM, the magnitude of NLOS error is much larger than that of multipath error, and the numerical stability of NLOS error is weaker than that of multipath error. With MHGM, the RMS of observation residuals with only multipath signals is reduced by 68.6%, while the RMS of observation residuals with NLOS signals is reduced by 80.9%. It shows that the MHGM can mitigate not only multipath error, but also most NLOS error. In addition, the modeling results of MHGM indicate that the NLOS error is positive, which is consistent with the theoretical error characteristics of NLOS signal.

After using MHGM, the accuracy of NLOS observations is still significantly lower than that of multipath observations. According to the propagation of uncertainty, we solve the accuracy difference between multipath and NLOS observations of station A, which is expressed as scale factor  $k$ , and propose two improved strategies based on strategy 0: strategy 1 of eliminating NLOS signal and strategy 2 of reducing its weight.

In the positioning test section, we solve the kinematic positioning results under different strategies and evaluate the improvements of strategies 1 and 2 compared with strategy 0. With multiple satellite systems, the improvements of strategy 1 in the horizontal and vertical directions are about 10%, while the improvements of strategy 2 are about 15–17%. With fewer satellite systems, strategy 1 of eliminating NLOS signals may lead to poor satellite geometry and cannot improve effectively, while strategy 2 of reducing the weight of NLOS signals is more robust. Since the strategy 2 can always improve the effectiveness of MHGM under the condition of different satellite systems in our test, it is more recommended.

**Table 3** Improvements of mean RMSE under strategies 1 and 2 compared with strategy 0 and mean number of available satellites under different satellite systems

| Satellite systems   | Strategy   | Improvements of mean RMSE compared with strategy 0 |                        | Mean number of available satellites |
|---------------------|------------|--|------------------------|-------------------------------------|
|                     |            | Horizontal direction (%)                           | Vertical direction (%) |                                     |
| GPS + BDS + Galileo | Strategy 1 | 10.3   | 11.0                   | 32.8                                |
|                     | Strategy 2 | 15.2   | 17.3                   |                                     |
| GPS + BDS           | Strategy 1 | 1.2  | 2.1                    | 27.4                                |
|                     | Strategy 2 | 8.2  | 11.3                   |                                     |
| BDS                 | Strategy 1 | 1.0  | -1.4                   | 19.0                                |
|                     | Strategy 2 | 4.7  | 11.9                   |                                     |
| GPS                 | Strategy 1 | -27.7  | -1.3                   | 8.4                                 |
|                     | Strategy 2 | 7.0  | 14.3                   |                                     |

The multipath error mitigation method we proposed is temporarily not applicable to the dynamic scenes. However, in static environments which need continuous observation and may have serious obstructions, such as dams and bridges, it can help to obtain real-time deformation information of millimeter level through kinematic positioning.

**Acknowledgements** We are very grateful to the reviewers and editor for their helpful remarks in improving the manuscript. This study is financially supported by the National Key Research and Development Program of China (Grant Nos. 2021YFC3000504, 2022YFB3904601).

**Data availability** The data analyzed during the current study are available from the corresponding author on reasonable request.

## References

- Agnew DC, Larson KM (2007) Finding the repeat times of the GPS constellation. *GPS Solut* 11(1):71–76. <https://doi.org/10.1007/s10291-006-0038-4>
- Bradbury J, Ziebart M, Cross PA, Boulton P, Read A (2007) Code multipath modelling in the urban environment using large virtual reality city models: determining the local environment. *J Navig* 60(1):95–105. <https://doi.org/10.1017/S0373463307004079>
- Cohen CE, Parkinson BW (1991) Mitigating multipath error in GPS-based attitude determination. In: Proceedings of the annual rocky mountain guidance and control conference, Keystone, CO, 2–6 February, pp 53–68
- Deng W, Ye J, Zhang T (2016) Acquisition and denoising algorithm of laser point cloud oriented to robot polishing. *Acta Optica Sinica* 36(08):180–188. <https://doi.org/10.3788/AOS201636.0814002>
- Dong D, Wang M, Chen W, Zeng Z, Song L, Zhang Q, Cai M, Cheng Y, Lv J (2016) Mitigation of multipath effect in GNSS short baseline positioning by the multipath hemispherical map. *J Geod* 90(3):255–262. <https://doi.org/10.1007/s00190-015-0870-9>
- Filippov V, Tatarnicov D, Ashjaee J, Astakhov A, Sutiagin I (1998) The first dual-depth dual-frequency choke ring. In: Proceedings of ION GNSS 1998, Nashville, USA, 15–18 September, pp 1035–1040
- Fuhrmann T, Luo X, Knöpfler A, Mayer M (2015) Generating statistically robust multipath stacking maps using congruent cells. *GPS Solut* 19(1):83–92. <https://doi.org/10.1007/s10291-014-0367-7>
- Groves PD, Adjrard M (2017) Likelihood-based GNSS positioning using LOS/NLOS predictions from 3D mapping and pseudoranges. *GPS Solut* 21(4):1805–1816. <https://doi.org/10.1007/s10291-017-0654-1>
- Groves PD, Jiang Z (2013) Height aiding,  $C/N_0$  weighting and consistency checking for GNSS NLOS and multipath mitigation in Urban areas. *J Navig* 66(5):653–669. <https://doi.org/10.1017/S0373463313000350>
- Hofmann-Wellenhof B, Lichtenegger H, Wasle E (2008) GNSS global navigation satellite systems: GPS, GLONASS, Galileo and more. Springer, Vienna, Austria
- Hsu LT (2018) Analysis and modeling GPS NLOS effect in highly urbanized area. *GPS Solut* 22(1):7. <https://doi.org/10.1007/s10291-017-0667-9>
- Hsu LT, Jan SS, Groves PD, Kubo N (2015) Multipath mitigation and NLOS detection using vector tracking in urban environments. *GPS Solut* 19(2):249–262. <https://doi.org/10.1007/s10291-014-0384-6>
- Jiang Z, Groves PD (2014) NLOS GPS signal detection using a dual-polarisation antenna. *GPS Solut* 18(1):15–26. <https://doi.org/10.1007/s10291-012-0305-5>
- Lau L, Cross P (2007) Development and testing of a new ray-tracing approach to GNSS carrier-phase multipath modelling. *J Geod* 81(11):713–732. <https://doi.org/10.1007/s00190-007-0139-z>
- Lu R, Chen W, Dong D, Wang Z, Zhang C, Peng Y, Yu C (2021) Multipath mitigation in GNSS precise point positioning based on trend-surface analysis and multipath hemispherical map. *GPS Solut* 25:119. <https://doi.org/10.1007/s10291-021-01156-5>
- Ragheb AE, Clarke PJ, Edwards SJ (2007) GPS sidereal filtering: coordinate- and carrier-phase-level strategies. *J Geod* 81(5):325–335. <https://doi.org/10.1007/s00190-006-0113-1>
- Tang W, Wang Y, Zou X, Li Y, Deng C, Cui J (2021) Visualization of GNSS multipath effects and its potential application in IGS data processing. *J Geod* 95(9):103. <https://doi.org/10.1007/s00190-021-01559-9>
- Tatarnikov D, Filippov V, Soutiaguine I, Astahov A, Stepanenko A, Shamatulsky P (2005) Multipath mitigation by conventional antennas with ground planes and passive vertical structures. *GPS Solut* 9(3):194–201. <https://doi.org/10.1007/s10291-004-0127-1>
- Wang L, Groves PD, Ziebart MK (2012) Multi-constellation GNSS performance evaluation for urban canyons using large virtual reality city models. *J Navig* 65(3):459–476. <https://doi.org/10.1017/S0373463312000082>
- Wang L, Groves PD, Ziebart MK (2013) GNSS shadow matching: improving urban positioning accuracy using a 3D city model with optimized visibility prediction scoring. *Navigation* 60(3):195–207
- Wang Z, Chen W, Dong D, Wang M, Cai M, Yu C, Zheng Z, Liu M (2019) Multipath mitigation based on trend surface analysis applied to dual-antenna receiver with common clock. *GPS Solut* 23:104. <https://doi.org/10.1007/s10291-019-0897-0>
- Wang Y, Zou X, Deng C, Tang W, Li Y, Zhang Y, Feng J (2020) A novel method for mitigating the GPS multipath effect based on a multi-point hemispherical grid model. *Remote Sens* 12(18):3045. <https://doi.org/10.3390/rs12183045>
- Xin S, Geng J, Zhang G, Ng H, Hsu LT (2022) 3D-mapping-aided PPP-RTK aiming at deep urban canyons. *J Geod* 96:78. <https://doi.org/10.1007/s00190-022-01666-1>
- Zhang Z, Li B, Gao Y, Shen Y (2019) Real-time carrier phase multipath detection based on dual-frequency C/N0 data. *GPS Solut* 23:7. <https://doi.org/10.1007/s10291-018-0799-6>

**Publisher's Note** Springer Nature remains neutral with regard to jurisdictional claims in published maps and institutional affiliations.

Springer Nature or its licensor (e.g. a society or other partner) holds exclusive rights to this article under a publishing agreement with the author(s) or other rightsholder(s); author self-archiving of the accepted manuscript version of this article is solely governed by the terms of such publishing agreement and applicable law.



**Xuan Zou** is an associate professor at the GNSS Research Center of Wuhan University. He obtained his Ph.D. degree from Wuhan University, P.R.C., in 2010. His current research mainly focuses on GNSS precise positioning technology.





**Ruinan Fu** is a Master at GNSS Research Center of Wuhan University. His current research mainly focuses on modeling multipath errors.



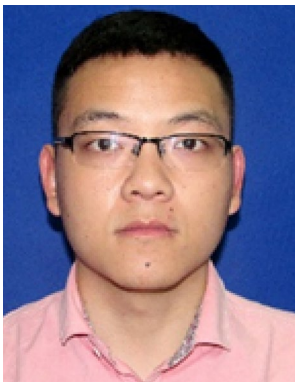
**Zhiyuan Li** is a Master at the GNSS Research Center of Wuhan University. His current research mainly focuses on GNSS precise positioning technology.



**Jian Tang** received a Ph.D. degree in Wuhan University. He is currently the Associate Professor of Wuhan University. His current research interests mainly focus on LiDAR SLAM and multi-source navigation.



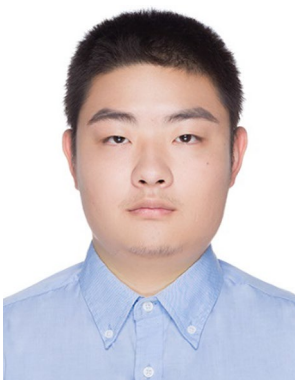
**Chenlong Deng** obtained his Ph.D. degree from Wuhan University in 2016, and he is currently an Associate Research Fellow at the GNSS Research Center. His research interests include multifrequency and multisystem data processing in precise positioning and integrity monitoring.



**Yawei Wang** is a Ph.D. candidate at the GNSS Research Center of Wuhan University. His current research mainly focuses on the GNSS multipath errors mitigation algorithm.



**Yangyang Li** is currently a post-graduate at the GNSS Research Center, Wuhan University. His current research interests include BDS/INS kinematic to kinematic positioning and data processing.



**Xiaoyun Fan** is currently pursuing a Ph.D. degree of Geodesy and Surveying and Mapping Engineering at the GNSS Research Center of Wuhan University. His research interests include multi-sensor SLAM, mobile mapping and automated driving.



**Weiming Tang** is currently a professor at Wuhan University. He obtained his Ph.D. degree with distinction in Geodesy and Engineering Surveying at the School of Geodesy and Geomatics in Wuhan University in 2006. His main research interests include network RTK and precise point positioning (PPP).